# Optical and electrical properties of InGaZnON thin films*

Jian Ke Yao(姚建可), Fan Ye(叶凡)†, and Ping Fan(范平)

*Shenzhen Key Laboratory of Advanced Thin Films and Applications, College of Physics and Energy, Shenzhen University, Shenzhen* 518060, *China*

(Received 29 August 2019; revised manuscript received 10 October 2019; accepted manuscript online 9 December 2019)

The substrate temperature ($T_s$) and $N_2$ partial pressure ($P_{N2}$) dependent optical and electrical properties of sputtered InGaZnON thin films are studied. With the increased $T_s$ and $P_{N2}$, the thin film becomes more crystallized and nitrified. The Hall mobility, free carrier concentration ($N_e$), and electrical conductivity increase with the lowered interfacial potential barrier during crystal growing. The photoluminescence (PL) intensity decreases with the increased $N_e$. The band gap ($E_g$) narrows and the linear refractive index ($n_1$) increases with the increasing concentration of N in the thin films. The Stokes shift between the PL peak and absorption edge decreases with $E_g$. The $n_1$, dispersion energy, average oscillator wavelength, and oscillator length strength all increase with $n_1$. The single oscillator energy decreases with $n_1$. The nonlinear refractive index and third order optical susceptibility increase with $n_1$. The Seebeck coefficient, electron effective mass, mean free path, scattering time, and plasma energy are all $N_e$ dependent.

**Keywords:** InGaZnON thin films, linear and nonlinear optical properties, Seebeck coefficient, electron effective mass

**PACS:** 81.05.Hd, 78.66.–w, 73.61.–r **DOI:** 10.1088/1674-1056/ab5fc1

## 1. Introduction

The InGaZnON (IGZON) thin films are now researched enormously as the active[1–3] or passivation[4] layers for thin film transistors to improve the stability.[5] The linear dispersive optical constants of IGZON thin films which are rarely studied till now are important to determine the sub-gap states in the thin films.[6–8] The structure of the crystalline IGZO thin film[9] is like that of the crystalline ZnO thin film which has non-centro symmetric structure with remarkable nonlinear optical response.[10,11] Generally, the third-order nonlinear optical susceptibility ($\chi^{(3)}$) and nonlinear refractive index ($n_2$) increase with linear refractive index ($n_1$).[12] The IGZO thin films have larger $n_1$ than the ZnO thin films,[8] indicating the better nonlinear optical response of the IGZO thin films. However, there are few experimental studies for the nonlinear optical properties of the IGZO thin films.[13] The nonlinear optical properties can also be theoretically investigated by the spectroscopy methods.[12,14,15] However, to our knowledge, there are none theoretical calculations done on the nonlinear optical properties of IGZO based thin films till now.

For accurate characterizing the electrical transport properties of the IGZON thin films, besides the free carrier concentration ($N_e$), Hall mobility ($\mu$), and electrical conductivity ($\sigma$), the effective mass of free carriers ($m_e^*$)[16] and scattering time ($\tau$)[17] should be determined together, but there are few related reports for the IGZON thin films. In this work, $m_e^*$ and $\tau$ for the IGZON thin films are extracted using the Seebeck coefficients $S$.

The substrate temperatures ($T_s$)[8,18] and $N_2$ partial pressures ($P_{N2}$)[1,7] during sputtering are crucial parameters determining the structure, composition, optical and electrical properties of thin films. Therefore, in this work, the $T_s$ and $P_{N2}$ dependent structure, composition, and optical and electrical properties of the IGZON thin films are investigated.

## 2. Experiment

The IGZON thin films were deposited by sputtering from an $InGaZnO_4$ target in diameter of 60 mm and thickness of 5 mm with the base pressure of $9.0 \times 10^{-4}$ Pa and the working pressure of 0.5 Pa. The IGZON1 to IGZON3 thin films were grown under the conditions of $Ar : N_2 : O_2$ flow rates of 40 : 5 : 5 sccm, RF power of 200 W, and $T_s$ of room temperature (RT), 300 °C, and 400 °C, respectively. And the IGZON4 to IGZON6 thin films were grown under the conditions of $Ar : N_2 : O_2$ flow rates of 40 : 10 : 0 sccm, RF power of 200 W, and $T_s$ of RT, 300 °C, and 400 °C, respectively. All the thin films have the thickness of ∼ 350 nm.

The structures of the thin films were studied by a Rigaku x-ray diffraction (XRD) meter. Cu $K\alpha$ radiation at the wavelength of 0.15418 nm was used as the x-ray source. The surface morphologies of the thin films were studied by a ZEISS Gemini scanning electron microscope (SEM). The surface chemical states of the thin films were characterized by a Thermo ESCALAB 250 x-ray photoelectron spectrometer (XPS) with a mono-chromate Al $K\alpha$ x-ray source of energy 1486.6 eV and x-ray spot size of 500 μm. The test was taken at the chamber pressure of 10 mbar. The XPS spectra were collected under the condition with pass energy of

*Project supported by the National Natural Science Foundation of China (Grant No. 61674107), Shenzhen Key Lab Fund, China (Grant No. ZDSYS 20170228105421966), and Science and Technology Plan of Shenzhen, China (Grant No. JCYJ20170302150335518).

†Corresponding author. E-mail: yefan@szu.edu.cn

 

20 eV and 0.05 eV/step for high-resolution scan. The low-energy electron flood gun with voltage of 3 V and current of 200 μA was applied to compensate the charging effects for the poor conductivity of the samples. The spectra were calibrated using the absorbed C 1s peak at 284.8 eV and fitted by Avantage software with Gaussian–Lorenzian curve with the shape of all peaks assumed to be 80% Gaussian and 20% Lorentzian. A smart mode was used to calculate the background. A Lambda 900 spectrometer was used to measure the transmittance of the thin films. To examine the defect states in the samples, the photoluminescence (PL, Edinburgh instrument, M300 Monochromator, Xe 900) spectroscopy was carried out at RT. To determine the optical constants and thickness of the thin films, the Spectroscopic ellipsometer (SE, Semilab GES5-E) was used. The carrier transportation properties and $S$ of the thin films were obtained by a Hall system using the van der Pauw configuration (HMS 2000) and an $S$ measuring apparatus (ZEM-3) at RT.

## 3. Results and discussion

The $T_s$ during deposition is a crucial process parameter which can determine the growth of crystalline IGZO (C-IGZO) based thin films. The C-IGZO thin films usually appear at optimal $T_s$ around 300 °C.[18] The IGZON thin films have minor N doping and therefore are still mainly IGZO based with similar texture and growth condition. Figure 1 and Table 1 show the XRD patterns and diffraction peaks parameters of the IGZON thin films. All thin films have the $C$-axis aligned crystal structure with (009) peak at 34°.[18] The (009) diffraction peak refers to $InGaZnO_4$ with hexagonal crystalline phase and $R$-3$m$ (166) space-group with unit cell $3.295 \times 3.295 \times 26.07$ $\langle 90.0° \times 90.0° \times 120.0° \rangle$ referred from PDF#38-1104 crystallographic card. The (009) peak of the crystalline thin films indicates the high degree of crystallinity exhibited by domains oriented perpendicular to the substrate. These lattice planes correspond to the alternating layers of indium oxide and gallium/zinc oxide in the unit cell. The crystal grain size ($G$) of the thin films is calculated by $G = 0.89\lambda/(B\cos\theta)$, where $\lambda$ is the wavelength of the x-ray (0.15418 nm), $\theta$ is the diffraction angle, and $B$ is the full width at half-maximum of the crystal plane. The peak intensity and $G$ slightly increase with $T_s$ at both $P_{N2}$, indicating the growing of the thin film crystal. With the increase of $T_s$, the mobility of atoms adsorbed on the surface of the substrate increases, therefore the deposited thin film has improved crystalline and packing density. Figure 2 shows the surface morphologies of the thin films. All thin films have nano-crystalline structures. The grain size increases with the increased $T_s$ and $P_{N2}$ during deposition. The results are consistent with the XRD results in Fig. 1. The increased $P_{N2}$ also increases $G$ of the thin films as revealed by comparing IGZON4 to IGZON6 with IGZON1 to IGZON3 thin films.

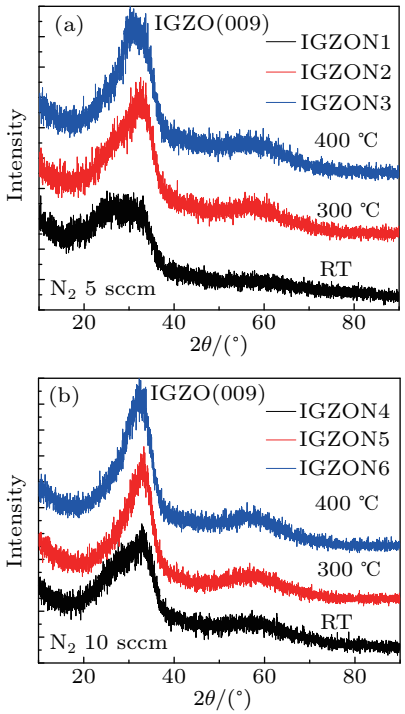


**Fig. 1.** XRD patterns of IGZON thin films deposited with increased $T_s$ from RT to 400 °C at $P_{N2}$ of (a) 10% and (b) 20%.

**Table 1.** The $d$, $2\theta$, $B$, and $I$ of the IGZO (009) peaks and $G$ of the IGZON thin films.

| Samples | $d$-spacing/Å | $2\theta/(°)$ | $B/(°)$ | Peak intensity/arb. units | $G$/nm |
|---|---|---|---|---|---|
| IGZON1 | 2.6935 | 33.235 | 0.425 | 247 | 14.3 |
| IGZON2 | 2.6885 | 33.299 | 0.288 | 318 | 28.5 |
| IGZON3 | 2.7434 | 32.613 | 0.578 | 346 | 35.2 |
| IGZON4 | 2.7161 | 32.950 | 0.121 | 238 | 38.1 |
| IGZON5 | 2.6885 | 33.299 | 0.288 | 318 | 39.4 |
| IGZON6 | 2.7434 | 32.613 | 0.578 | 346 | 40.1 |

The XPS spectra of O 1s and N 1s are shown in Fig. 3. The Gaussian fitting is used for fitting the combined O 1s peaks. The resulting sub-peaks at the binding energies of 530.3 eV, 530.9 eV, and 533.2 eV are attributed to $O^{2-}$ surrounded by metal atoms, oxygen vacancies ($V_O$), and $OH^{-1}$ impurities, respectively, at Figs. 3(a) and 3(b).[2] The signals of Ga Auger at 396.7 eV and Ga–N bonds at 397.8 eV are observed in Figs. 3(c) and 3(d).[2] The atomic ratios of $V_O$ and N are calculated. It can be found that the concentration of $V_O$ ($C_{VO}$, at.%) decreases with $T_s$ at $P_{N2}$ of 10% (Fig. 3(a)) due to the increased oxidation at higher $T_s$. At $P_{N2}$ of 20% (Fig. 3(d)), with the increased $T_s$, the nitridation is slightly increased. With the concentration of N ($C_N$, at.%) slightly increased with the increase of $T_s$, $C_{VO}$ also increases, which indicates the less oxidation than nitridation in the thin films, the less oxidation is also due to the oxygen escaping by the M–O bonds breaking during the deposition at higher temperature. The $C_N$ slightly increases with $T_s$ and $P_{N2}$ by the increased nitridation at higher $T_s$ and $P_{N2}$. At the same $T_s$, by comparing IGZON1 with IGZON4, IGZON2 with IGZON5, and IGZON3 with IGZON6, the thin films have larger $C_N$ and $C_{VO}$ by the slightly increased nitridation and decreased oxidation with the increased $P_{N2}$.

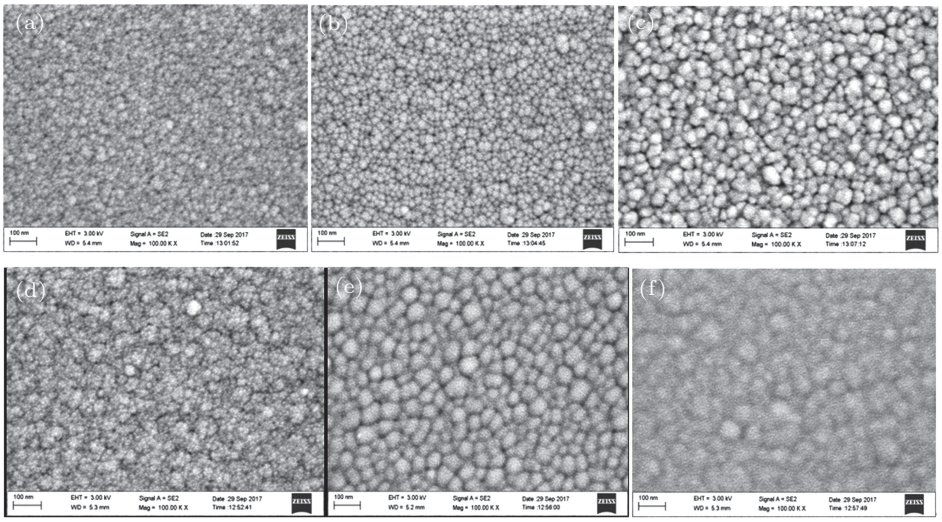


**Fig. 2.** The SEM surface morphologies with $10^5$ magnification of the IGZON thin films deposited at (a) $T_s$ of RT, $P_{N2}$ of 10%; (b) $T_s$ of 300 °C, $P_{N2}$ of 10%; (c) $T_s$ of 400 °C, $P_{N2}$ of 10%; (d) $T_s$ of RT, $P_{N2}$ of 20%; (e) $T_s$ of 300 °C, $P_{N2}$ of 20%; (f) $T_s$ of 400 °C, $P_{N2}$ of 20%.

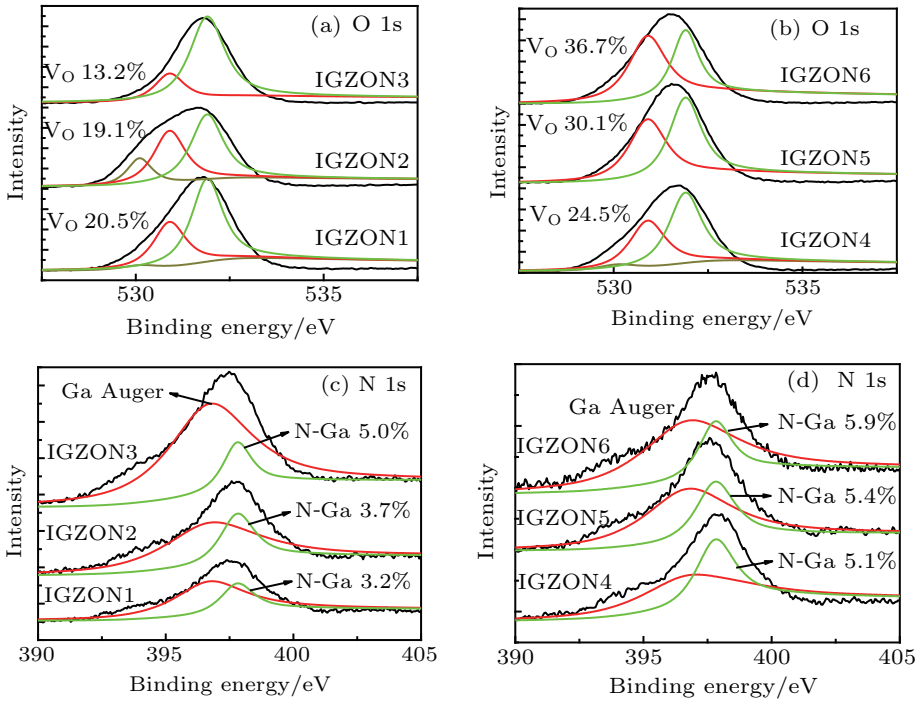


**Fig. 3.** The O 1s XPS spectra of IGZON thin films deposited at (a) $P_{N2}$ of 10% and $T_s$ of RT, 300 °C, and 400 °C; (b) $P_{N2}$ of 20% and $T_s$ of RT, 300 °C, and 400 °C. N 1s XPS spectra of IGZON thin films deposited at (c) $P_{N2}$ of 10% and $T_s$ of RT, 300 °C, and 400 °C; (d) $P_{N2}$ of 20% and $T_s$ of RT, 300 °C, and 400 °C.

The stokes shifts between the RTPL spectra excited by 325 nm laser and the absorption coefficients are shown in Fig. 4. The optical absorption coefficient $\alpha$ is defined as[19]

$$\alpha = -\frac{1}{d}\ln\left[\frac{T}{(1-R)^2}\right], \tag{1}$$

where $T$ is the transmittance, $R$ is the reflectance measured by the spectrometer as shown in Fig. 6, and $d$ is the thickness of the thin film. The thin films exhibit broad and asymmetric PL spectra extended from UV to visible region with two peaks centered at 405 nm (3.06 eV) and 437 nm (2.84 eV).[20] The main violet emission peak centered at 3.06 eV is attributed to the electron transition from conduction band tail states to valence band tail states.[20] The minor blue emission at 2.84 eV is ascribed to the electron transition from interstitial to vacancy zincs. The PL intensity of the near-band-edge (NBE) emission strongly depends on the free carrier concentration ($N_e$) in the thin films. All IGZON thin films are n-type semiconductor. The $N_e$ in the thin films increases with $T_s$ and $P_{N2}$ during deposition as seen in Fig. 5(a), which is due to the reduced crystal interfacial barriers with the increased size of the crystal grains in the thin films. As $N_e$ increases, the PL intensity at 405 nm peak decreases. The PL and absorption spectra are compared. Between the two spectra, there exists a Stokes shift which is related to many effects such as electron–phonon coupling, lattice distortions, and interface and point defects.[21] The decrease of the Stokes shift as listed in Table 2 is ascribed

to the narrowing of the band gap ($E_g$) as seen later in Figs. 7(g) and 7(h).

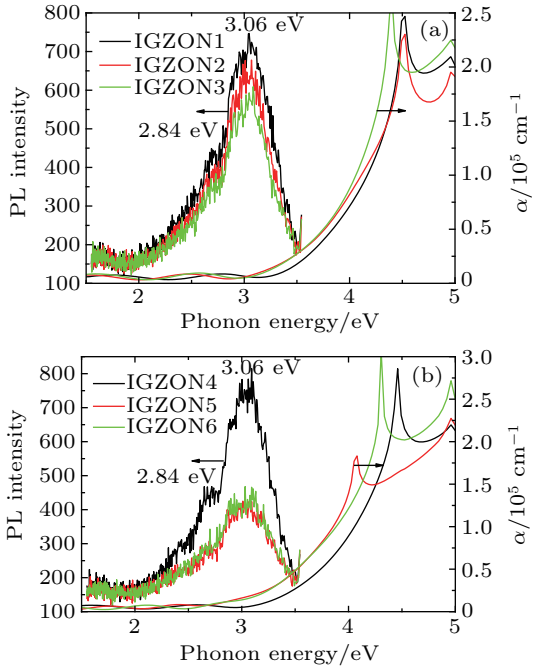


**Fig. 4.** The stokes shift between RTPL and absorption spectra for IGZON thin films deposited at $T_s$ of RT, 300 °C, 400 °C and (a) $P_{N2}$ of 10% or (b) $P_{N2}$ of 20%.

The measured $\sigma$, $\mu$, and $S$ of the thin films are shown in Figs. 5(a) and 5(b). It is found that the $T_s$ and $P_{N2}$ have substantial influences on the charge transportation properties. The $\sigma$ and $\mu$ increase with $T_s$ and $P_{N2}$ for the reduced interfacial crystal barrier by the increased crystalline size. The $S$ depends on the temperature and electron effective mass ($m_e^*$) at the Fermi level and $N_e$ as[22]

$$S = \frac{8\pi^2 k_B^2 T}{3qh^2} m_e^* \left(\frac{\pi}{3N_e}\right)^{2/3}, \tag{2}$$

where $k_B$ is the Boltzmann constant, $q$ is the electron charge, and $h$ is the Plank constant. All thin films have negative $S$ at RT, indicating the n-type conductivity. The $S$ increases with $N_e$ obeying well the relation (3), from which $m_e^*$ can be calculated as shown in Fig. 5(b). For the IGZO thin film with $N_e$ of $3.5 \times 10^{20}$ cm$^{-3}$, the $m_e^*$ is calculated to be 0.30 $m_e^0$, where $m_e^0$ is the static mass of electron.[23] The $m_e^*$ increases with $N_e$ for the non-parabolicity of the conduction band, which shows the validity of our result. For accurate characterizing the transportation properties, the free electron mean path ($l_e$) and scattering time ($\tau$) are calculated by[24,25]

$$l_e = \frac{h}{2q}\left(\frac{3N_e}{\pi}\right)^{1/3}\mu, \tag{3}$$

$$\tau = \frac{m_e^*\mu}{q}, \tag{4}$$

where $\mu$ is the Hall mobility. The results are shown in Fig. 5(c). The smaller $l_e$ than the crystal grain size in Table 1 indicates that the grain boundaries have no significant effects on the electrical transport properties. The $l_e$ and $\tau$ are both $N_e$ and $\mu$ co-dependent.

Figure 6 shows the transmittance and reflectance spectra of the IGZON thin films. All thin films are transparent in the visible region. The transmittance slightly decreases with $T_s$ in the infrared region by free carrier absorption with the increased $N_e$.

The linear refractive index and dielectric constants are fitted by the SE method based on Cauchy and Drude models.[23] Figures 7(a) and 7(b) show that $n_1$ increases with $T_s$ and $P_{N2}$. There are two mechanics for the increase of $n_1$. One is the increased crystal quality and packing density with the increased mobility of atoms adsorbed on the surface of the substrate at higher $T_s$. The other is the increased polarizability by N doping for the larger atomic radius of N than that of O.

The dispersion and absorption of dielectrics are represented by the empirical formula[26,27]

$$\varepsilon^* - \varepsilon_\infty = (\varepsilon_0 - \varepsilon_\infty)/[1 + (i\omega\tau_0)^{1-\alpha}], \tag{5}$$

where $\varepsilon^*$ is the complex dielectric constant, $\varepsilon_0$ and $\varepsilon_\infty$ are the static and high frequency dielectric constants, $\omega$ equals $2\pi$ times the frequency, and $\tau_0$ is the generalized relaxation time. The parameter $\alpha$ can assume values between 0 and 1, the former giving the result of Debye for polar dielectrics. Figures 7(c) and 7(d) show the calculated real and imaginary dielectric constants ($\varepsilon_1$ and $\varepsilon_2$), that is the Cole–Cole plots, from which $\varepsilon_\infty$ is determined at the interception of the real axis.

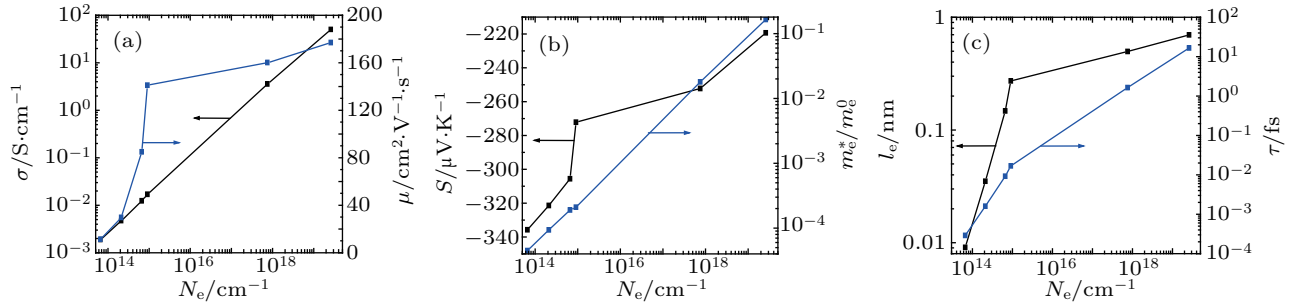


**Fig. 5.** The relation of (a) electrical conductivity ($\sigma$), Hall mobility ($\mu$), (b) Seebeck coefficients ($S$), effective electron mass ($m_e^*/m_e^0$), (c) free electron mean path ($l_e$), and scattering time ($\tau$) with $N_e$.

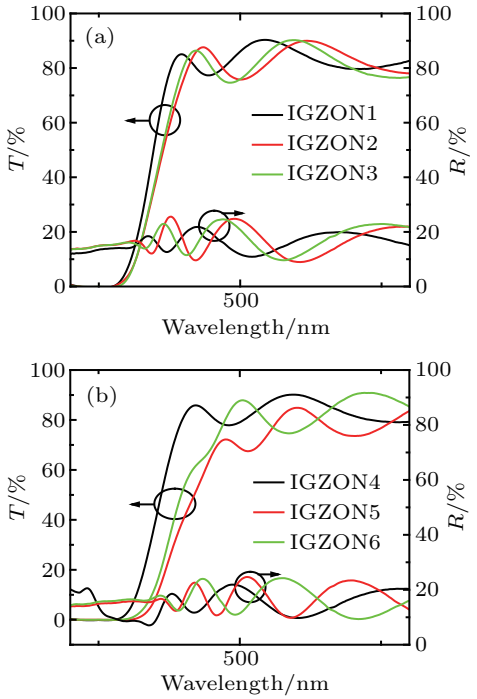


**Fig. 6.** The transmittance and reflectance spectra of IGZON thin films deposited at $T_s$ of RT, 300 °C, 400 °C and (a) $P_{N2}$ of 10% or (b) $P_{N2}$ of 20%.

The onset of free carrier absorption is given by the plasma energy[28]

$$E_p = \left(\frac{h^2 q^2 N_e}{4\pi^2 m_e^* \varepsilon_\infty \varepsilon_0}\right)^{1/2}, \tag{6}$$

Figure 7(i) shows that $E_p$ increases with $N_e$. It is known that the exponential optical energy dependence of $\alpha$ in the vicinity of the band gap can be described by[29]

$$\alpha \propto \exp\left(\frac{E}{E_u}\right), \tag{7}$$

where $E$ is the photon energy and $E_u$ is the Urbach energy related to the joint density of states determined by both conduction and valence band tail states. The extracted $E_u$ is shown in Figs. 7(e) and 7(f). By assuming the parabolic densities of band states within IGZON, $E_g$ is extracted by the Tauc method[30]

$$(E\alpha)^{1/2} = B(E - E_g), \tag{8}$$

where $B$ is the slope. In Figs. 7(g) and 7(h), it is found that $E_g$ is narrowed with the increase of $T_s$ and $P_{N2}$ during deposition for the IGZON thin films. The increases of $T_s$ and $P_{N2}$ during deposition have increased $C_N$ in the IGZON thin films as seen in Figs. 3(c) and 3(d). As discussed by Ryu, with the increased $C_N$ in thin films, the band gap decreases from 3.4 eV, 1.3 eV to 1.1 eV for ZnO, ZnON, and $Zn_2N_3$ thin films, respectively, which is mainly due to the N states in the valence band.[31] Therefore, in the IGZON thin films with the increase of $C_N$, $E_g$ is narrowed. Although the free carrier concentration in the IGZON thin films is increased with the increase of $T_s$ and $P_{N2}$ during deposition as seen in Fig. 5(a). The band gap will widen with the increase of $N_e$ due to the Burstein–Moss (BM) effect.[32] The electron–electron and electron–ion scatterings will also narrow the band gap. Here, the band gap narrowing by the increase of $C_N$ in the thin films and by the electron–electron and electron–ion scatterings may be larger than the band gap widening by the BM effect. Therefore, for the IGZON thin films, with the increase of $T_s$ and $P_{N2}$ during deposition, $E_g$ is narrowed.

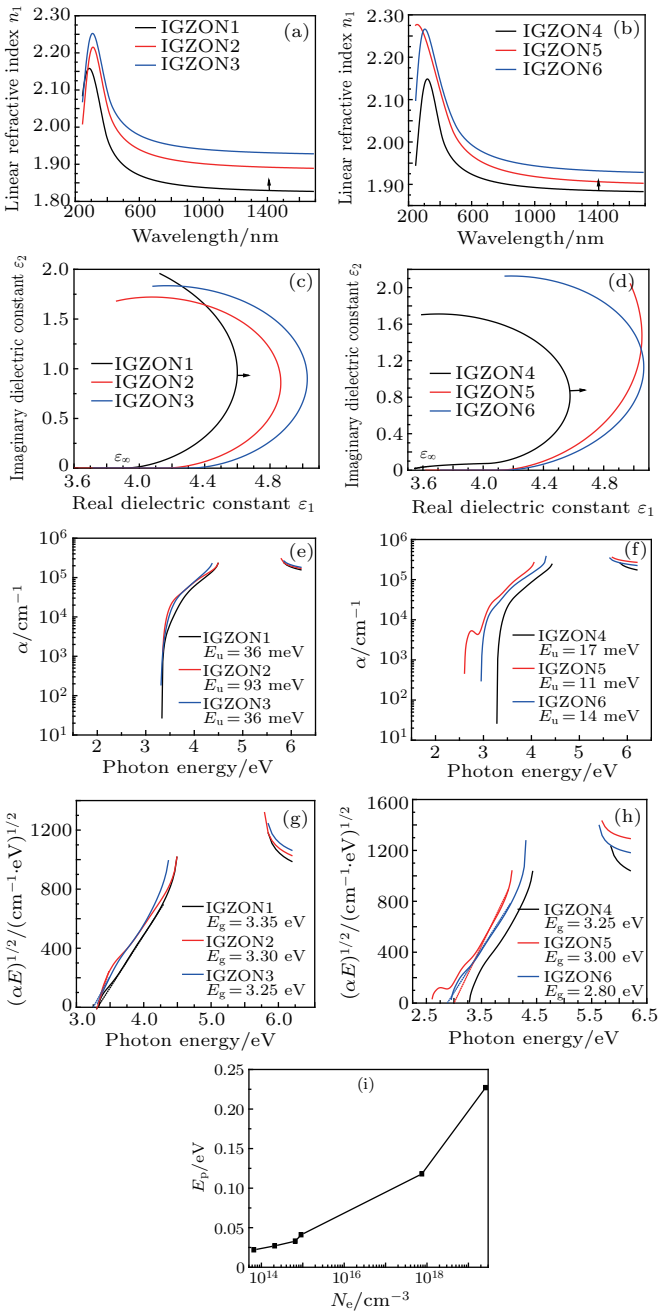


**Fig. 7.** (a), (b) Linear refractive index ($n_1$); (c), (d) Cole–Cole plots of dielectric functions; (e), (f) absorption coefficients ($\alpha$); (g), (h) band gap ($E_g$); and (i) relation of plasma energy ($E_p$) with $N_e$ for IGZON thin films.

The spectral dependent linear refractive index dispersion can be evaluated by the single-effective-oscillator model proposed by Wemple-Didomenico.[33] The $n_1$ of thin films can be

related with oscillator energy ($E_o$) and dispersion energy ($E_d$) by[33]

$$n_1^2 - 1 = \frac{E_o E_d}{E_o^2 - (h\nu)^2}, \tag{9}$$

where $h\nu$ is the photon energy, $E_o$ and $E_d$ are the single oscillator constants. $E_o$ is the average excitation energy for electronic transitions and $E_d$ is the dispersion energy which is a measure of the strength of inter-band optical transitions. This model describes the dielectric response for transitions below the optical gap. It plays an important role in determining the behavior of $n_1$. Figures 8(a) and 8(b) show the optical dispersion behavior of $(n_1^2-1)^{-1}$ vs. $(h\nu)^2$ for the IGZON thin films. The oscillator parameters $E_o$ and $E_d$ are determined by fitting a straight line to the points. The slope of the linear relation represents $(E_o E_d)^{-1}$ and the interception with the vertical axis equals to $E_o/E_d$. The increased values of $E_o$ and $E_d$ as listed in Table 2 indicate the improved structure order of the thin films with $T_s$ and $P_{N2}$. The static refractive index $n_s$ can be determined by[34]

$$n_s = (1 + E_d/E_o)^{1/2}. \tag{10}$$

**Table 2.** Optical and dispersion energy parameters for IGZON thin films.

| Samples | 1 | 2 | 3 | 4 | 5 | 6 |
|---|---|---|---|---|---|---|
| Stokes shift/eV | 1.6 | 1.5 | 1.5 | 1.5 | 1.3 | 1.1 |
| $E_o$/eV | 8.130 | 7.596 | 7.594 | 7.172 | 6.752 | 6.718 |
| $E_d$/eV | 16.679 | 17.541 | 18.249 | 19.476 | 20.524 | 20.582 |
| $\lambda_0$/nm | 4.8 | 4.8 | 4.9 | 4.9 | 5.1 | 5.3 |
| $S_0$/nm$^{-2}$ | 0.10 | 0.10 | 0.11 | 0.11 | 0.12 | 0.14 |
| $n_s$ | 1.824 | 1.879 | 1.889 | 1.900 | 1.924 | 1.924 |
| $\varepsilon_s$ | 3.327 | 3.531 | 3.568 | 3.610 | 3.702 | 3.702 |
| $\varepsilon_\infty$ | 4.0 | 4.2 | 4.4 | 3.6 | 4.1 | 4.2 |

The static dielectric constant ($\varepsilon_s$) is estimated by $\varepsilon_s = n_s^2$.[33] It is observed that $n_s$ and $\varepsilon_s$ almost increase with $T_s$ and $P_{N2}$. The refractive index can also be analyzed to determine the average oscillator wavelength ($\lambda_0$) and oscillator length strength ($S_0$) for the thin films. To obtain these values, the single term Sellmeier oscillator is used as[33]

$$n_1^2 - 1 = \frac{S_0 \lambda_0^2}{1 - \lambda_0^2/\lambda^2}. \tag{11}$$

The $\lambda_0$ and $S_0$ values are obtained by the linear parts of $1/(n_1^2-1)$ vs. $\lambda^{-2}$ (not shown here), and the results are summarized in Table 2.

It is known that the induced dielectric polarization ($P$) depends on the applied electrical field ($E$) which can be expressed in a series of powers of $E$ as[11]

$$P = \chi E + \chi^{(2)} E^2 + \chi^{(3)} E^3, \tag{12}$$

where $\chi^{(1)}$, $\chi^{(2)}$, and $\chi^{(3)}$ represent the linear, second, and third order nonlinear optical susceptibilities, respectively. The refractive index $n(\lambda)$ can be expressed as[11]

$$n(\lambda) = n_1(\lambda) + n_2(\lambda), \tag{13}$$

where $n_1(\lambda)$ and $n_2(\lambda)$ are the linear and nonlinear refractive indexes, respectively. The $\chi^{(1)}$ and $\chi^{(3)}$ are calculated by[11]

$$\chi^{(1)} = (n_1^2 - 1)/4\pi, \tag{14}$$

$$\chi^{(3)} = A[\chi^{(1)}]^4, \tag{15}$$

where $A$ equals to $1.7 \times 10^{-10}$ esu. The $n_2$ is calculated by[11]

$$n_2 = 12\pi\chi/n_1. \tag{16}$$

It is found that both the linear and nonlinear optical properties of the thin films enhance with $T_s$ and $P_{N2}$ during deposition. The $\chi^{(1)}$, $\chi^{(3)}$, and $n_2$ all increase and follow the same variation trend of $n_1(\lambda)$ for the improved crystalline and structural order and the increased $C_N$ as seen in Figs. 8(c)–8(h).

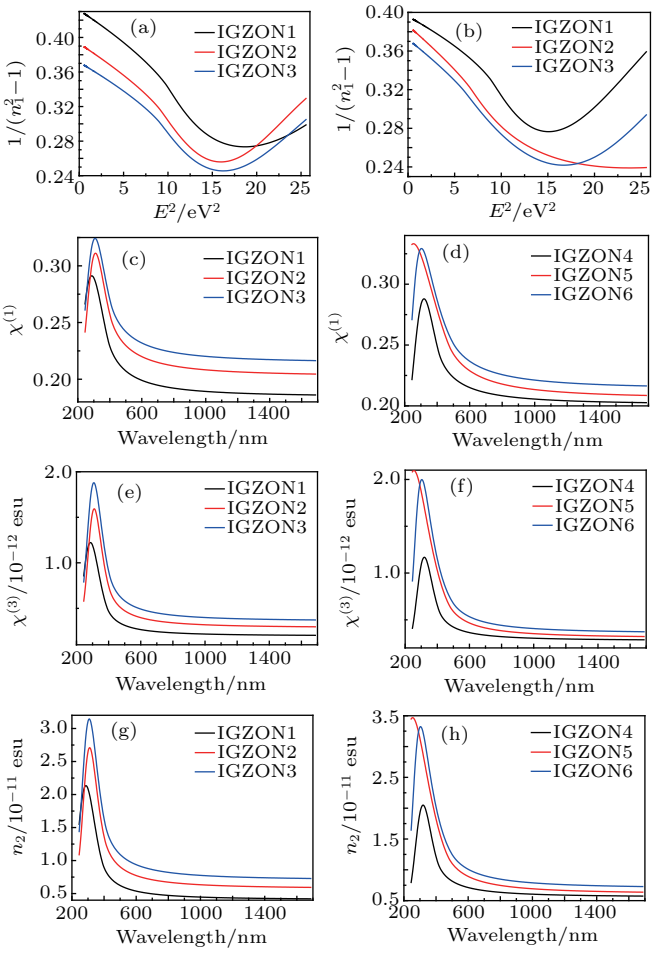


**Fig. 8.** The (a), (b) $(n^2-1)^{-1}$ vs. $(h\nu)^2$, (c), (d) $\chi^{(1)}$, (e), (f) $\chi^{(3)}$, and (g), (h) $n_2$ for IGZON thin films.

## 4. Conclusion and perspectives

The increase of $T_s$ and $P_{N2}$ during sputtering mainly enhances the crystallization which lowers the interfacial crystal potential barrier and therefore increases the $\mu$, $N_e$, and $\sigma$ of the IGZON thin films. The $S$, $m_e^*$, $\tau$, $l_e$, and $E_p$ are all increase with $N_e$. The increase of $T_s$ and $P_{N2}$ enhances the nitrification of the IGZON thin films. The $n_1$, $n_2$, $\chi^{(1)}$, and $\chi^{(3)}$ all increase with the improved crystallization and nitrification of the thin

films. The $E_o$ decreases with the increase of $n_1$. The $E_d$, $\lambda_0$, and $S_0$ increase with the increase of $n_1$. The $E_g$ narrows by the increased $C_N$ which counteracts the widening effect by the increased $N_e$.

## References


[1] Liu P T, Chang C H, Fuh C S and Sze S M 2016 *J. Disp. Technol.* **12** 1070

[2] Huang X M, Wu C F, Lu H, Ren F F, Chen D J, Zhang R and Zheng Y D 2013 *Appl. Phys. Lett.* **102** 193505

[3] Raja J, Jang K, Balaji N, Choi W, Trinh T T and Yi J S 2013 *Appl. Phys. Lett.* **102** 083505

[4] Liu P T, Chou Y T, Teng L F, Li F H, Fuh C S and Shieh H P D 2011 *IEEE Elec. Dev. Lett.* **32** 1397

[5] Kamiya T, Nomura K and Hosono H 2010 *Sci. Technol. Adv. Mater.* **11** 044305

[6] Kamiya T, Nomura K and Hosono H 2009 *J. Disp. Technol.* **5** 468

[7] Chen X, He G, Lv J, Liu M, Wang P, Chen X and Sun Z 2015 *J. Alloy. Compd.* **647** 1035

[8] Chen X F, He G, Gao J, Zhang J W, Xiao D Q, Jin P and Deng B 2015 *J. Alloy Compd.* **632** 533

[9] Yamazaki S, Koyama J, Yamamoto Y and Okamoto K 2012 *Society of Information Display Gigest* **183**

[10] Djuris A and Leung Y 2006 *Small* **2** 944

[11] Larciprete M and Centini M 2015 *Appl. Phys. Rev.* **2** 031302

[12] Malik G, Jaiswal J, Mourya S and Chandr R 2017 *J. Appl. Phys.* **122** 143105

[13] Sanal K, Vishnu K, Shijeesh M R and Jayaraj M K 2014 *Proc. SPIE* **9161** 91611B

[14] Shaaban E, El-Hagary M, Moustafa E, Hassan H, Ismail1 Y, EmamIsmail M and Ali A 2016 *Appl. Phys. A* **122** 20

[15] Jilani A, Abdel-wahab M, Zahran H, Yahia I and Al-Ghamdi A 2016 *Appl. Phys. A* **122** 862

[16] Wang Y Q, Zhu J H and Tang W 2014 *Appl. Phys. Lett.* **104** 212103

[17] Tang J, Deng L Y, Tay C B, Zhang X H, Chai J W, Qin H, Liu H W, Venkatesan T and Chua S J 2014 *J. Appl. Phys.* **115** 033111

[18] Lynch D, Zhu B, Levin B, Muller D, Ast D, Greene R and Thompson M 2014 *Appl. Phys. Lett.* **105** 262103

[19] Cai P G, Zhen D, Xu X J, Liu Y L, Chen N B, Wei G R and Sui C H 2010 *Mater. Sci. Eng. B* **171** 116

[20] Tiwari N, Chauhan R, Shieh H P D, Liu P T and Huang Y 2016 *IEEE Elec. Dev. Lett.* **63** 1578

[21] Sagara P, Shishodia P, Mehraa R, Okada H, Wakahara A and Yoshida A 2007 *J. Lumin.* **126** 800

[22] Korotcenkov G, Brinzari V and Ham M 2018 *Crystals* **8** 1

[23] Takagi A, Nomura K, Ohta H, Yanagi H, Kamiya T, Hirano M and Hosono H 2005 *Thin Solid Films* **486** 38

[24] Wang Y Q, Zhu J H and Tang W 2014 *Appl. Phys. Lett.* **104** 212103

[25] Tang J, Deng L Y, Tay C B, Zhang X H, Chai J W, Qin H, Liu H W, Venkatesan T and Chua S J 2014 *J. Appl. Phys.* **115** 033111

[26] Volintiru I, Creatore M and Sanden M 2008 *J. Appl. Phys.* **103** 033704

[27] Cole K S and Cole R H 1941 *J. Chem. Phys.* **9** 341

[28] Cole K S and Cole R H 1942 *J. Chem. Phys.* **10** 98

[29] Hamberg I and Granqvist C 1986 *J. Appl. Phys.* **60** R123

[30] Tharayila N, Sagarb S, Raveendrana R and Vaidyan A 2007 *Physica B* **399** 1

[31] Ryu M, Kim T S, Son K S, Kim H S, Park J S, Seon J B, Seo S J, Kim S J, Lee E, Lee H, Jeon S H, Han S and Lee S Y 2012 *IEEE International Electron Devices Meeting* **112**

[32] Hamberg I and Granqvist C 1986 *J. Appl. Phys.* **60** R123

[33] Fung T C, Chuang C S, Nomura K, Shieh H P D, Hosono H and Kanicki J 2008 *J. Inform. Disp.* **9** 21

[34] Yakuphanoglu F, Cukurovali A and Yilmaz I 2004 *Physica B* **351** 53